İSTANBUL UNIVERSITY CERRAHPAŞA

ORIGINAL ARTICLE
Electrica 2024; 24(2): 336-345

Finite Set-Model Predictive Control for Modified quasi Switched Z Source Level 3 Off-board Charger for Active Power Oscillations Damping in Weak Grids

Anish Tiwari, Anandita Chowdhury

Sardar Vallabhbhai National Institute of technology-Surat, Gujarat, India

Cite this article as: A. Tiwari and A. Chowdhury, "Finite set-model predictive control for modified switched Z source level 3 off-board charger for active power oscillations damping in weak grids," *Electrica*, 24(2), 336-345, 2024.

ABSTRACT

Integrating renewables into compact Electric Vehicle charging networks poses challenges like voltage imbalances and power oscillations. A recent study tackled these with a novel control strategy for a three-phase modified switched Z source grid-tied converter. Unlike traditional methods using oversized capacitors, this study employed extra proportional integral (PI) control loops to eliminate negative sequence components. Simulation results showcased the potential of the finite set-model predictive control (FS-MPC) in reducing Direct Current-Link variations from double-frequency ripples. The removal of redundant PI control loops also boosted control unit efficiency. The study introduced an improved modified switched Z source design, refining control logic. The predictive control algorithm effectively mitigated active power oscillations without extensive gain tuning, even with unbalanced grids, ensuring IEEE 519™-2014 compliance. This research addresses power quality concerns in EV charging infrastructure, offering a practical solution for stable and efficient operations. By adopting the FS-MPC strategy and integrating the modified switched Z source design, the study optimizes power flow and enhances EV charging reliability.

Index Terms—Active power oscillations, finite set predictive control algorithm, modified switched quasi-Z source converter, power quality, Pulse Width Modulation, weak grid

Corresponding author:
Anish Tiwari

E-mail:
anishtiwari283@gmail.com

Received: June 18, 2023

Revision Requested: August 19, 2023

Last Revision Received: November 21, 2023

Accepted: January 4, 2024

Publication Date: April 17, 2024

DOI: 10.5152/electrica.2024.23081

I. INTRODUCTION

Increasing energy demand requires integrating renewable sources reducing emissions versus traditional facilities [1]. However, this strains alternators, demanding precise voltage and frequency control, raising costs, and shortening lifespan. Renewable variability necessitates backup power to prevent failures [2], stressing the importance of continuous power. These issues lead to problems like frequency deviations, voltage fluctuations, harmonic distortion, and flickering, endangering system stability if unaddressed [3].

Unbalanced voltage concerns in AC microgrids diminish power quality and hasten battery deterioration according to article [4]. Without battery storage, renewable sources fail to supply peak demand unless peak hours coincide with their operation [5-7]. Researchers in [8] improve dependability by simplifying power conversion. The fundamental impedance source network converter with buck-boost capabilities has promise for a wide range of power applications. This circuit, which employs an X-shaped network with two inductors, two capacitors, and six power switches in an H-bridge arrangement, outperforms traditional boost converters in terms of reliability and cost-effectiveness [9].

Article [10] explores the bidirectional capabilities of the quasi-modified switched Z-source inverter (Bi-q MSZSI) versus the conventional bidirectional quasi-Z-source inverter (Bi-q ZSI). It focuses on improving power exchange between the electrical grid and energy storage, especially for uninterrupted power flow (UPF) and grid support, emphasizing the advantages of Bi-q MSZSI, especially under balanced grid conditions. It can maintain a constant DC-link with a lower duty ratio, allowing more modulation index adjustments without compromising bidirectional functionality. The Bi-q MSZSI excels at regulating power exchange between batteries and the grid, supporting reactive power demands. However, it requires complex control systems and may suffer efficiency losses in bidirectional power conversion. Conversely, the proposed finite-set model

predictive control (FS-MPC) simplifies control, eliminating extra proportional integral (PI) loops, even under non-ideal grid conditions, significantly reducing overall control complexity, a notable advancement in control technique.

Laib, Krim, Talbi, et al. [11] used FS-MPC for large-scale grid-connected PV systems, enhancing power point tracking with variable solar irradiation. They employed rapid voltage-oriented maximum power point tracking via FS-MP current controller (FS-MPCC) to boost energy extraction. Their FS-MPC algorithm centralized control for the grid-connected five-level neutral point clamped (NPC) inverter, ensuring superior control with improved grid current quality, DC-link capacitor voltage balance, and overall system robustness versus conventional methods. Liming Liu, Hui Li, Yaosuo Xue, Wenxin Liu et al. [12] address large-scale grid-connected PV system challenges using cascaded modular multilevel converters. They propose a decoupled active and reactive power control strategy, ensuring efficient power distribution. Simulations confirm its effectiveness in maintaining power quality and stability in cascaded PV systems.

Yaramasu et al. [13] propose model predictive control for high-power wind energy systems, specifically four-level diode-clamped inverters. Their approach regulates DC-link voltage, fulfills grid operator reactive power demands, balances capacitors, and minimizes switching frequency. It selects optimal states via a cost function derived from a discrete-time model, maintaining a 750–850 Hz switching frequency. Validation is conducted through simulations and experiments using the dSPACE DS1103 platform. Yaramasu et al. [14] present model-predictive control for a high-power wind energy conversion system's medium voltage, grid-tied four-level diode-clamped inverter. It regulates DC-link voltage, fulfills reactive power needs, and balances DC-link capacitor voltages. Using a discrete-time model, it predicts grid currents and DC-link voltages for switching states, choosing the optimal state via a cost function. Demonstrated in simulations and experiments, it maintains a 750–850 Hz switching frequency.

Level 3 commercial fast charging transforms EV charging, delivering rapid 1-hour charging at highway rest areas and urban refueling points, utilizing a 480 V or higher voltage three-phase circuit. Yet residential implementation faces hurdles due to installation costs ($30 000 to $160 000) and upkeep. Public stations employ level 2 or level 3 chargers for fast charging but must manage local distribution equipment during peak periods. To solve these issues, integrating controlled smart charging systems and reliable communication networks remains vital for seamless EV integration [15].

The study [16] assesses the Bi-q-MSZSI topology for Vehicle-to-Grid integration by comparing conventional PI control involving multiple cascaded PI controllers on both the DC and AC sides, requiring sophisticated tuning with hybrid FS-MPC control utilizing a single PI controller on the DC side that reduces control complexity. The bi-q-MSZSI topology with FS-MPC demonstrates superior performance over PI control as it addresses oscillation issues potentially extending battery life by improving transient peak amplitudes and reducing switching ripples in the battery current.

The article's key contributions are as follows:

1. The predictive control algorithm successfully mitigates double-frequency 2ω power oscillations at the DC link, outperforming conventional PI control.
2. It significantly reduces computational complexity, employing a single-step optimization across the prediction horizon instead of multiple control loops.
3. The algorithm markedly decreases current distortion levels, achieving levels well within IEEE 519™-2014 standards. These contributions highlight the article's advancements in addressing power oscillations, reducing complexity, and ensuring compliance with distortion standards.

II. SYSTEM DESCRIPTION

Unbalanced grid voltages in MSZS level 3 chargers cause double-frequency ripples in EV DC-links. Solutions include increased DC-link capacitance or classic control based on instantaneous power theory. Generating current references with both positive and negative sequence components minimizes active power oscillations from unbalanced grid voltages. However, more control loops raise complexity. The proposed predictive control minimizes DC-link voltage ripples without added complexity. Fig. 1 depicts the AC microgrid connection and bidirectional Modified quasi Switched Z Source (MSQSZ) structure for applications like interleaved battery chargers

In the Z source setup of the AC microgrid, the inductor plays a pivotal energy storage role, offering substantial boosting capability. To avert inductor core saturation, a high-boost converter with a reduced duty range is required. Two approaches exist: one involves a cascaded boost topology, like the hybrid 3-Z boost topology, incorporating extra diodes and passive elements [17]. The other employs a switched quasi Z-source boost converter (SQZC) with active components and diodes, providing high boosting with a narrower duty range. However, SQZC requires a constant DC-link input due to the shoot-through state, limiting its suitability. Modifications in the SQZS configuration [18] resolve this, allowing for a constant DC-Link and high boost, as shown in Fig. 2. This setup has promising potential for reliable battery charging and extended lifespan.

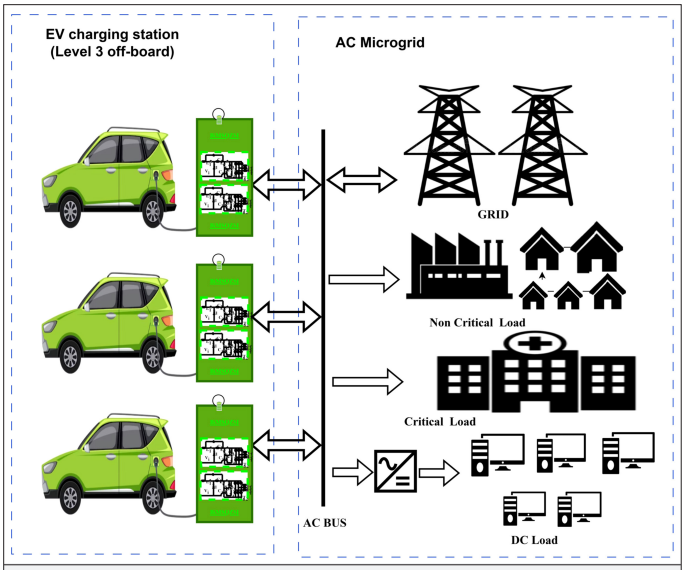

Fig. 1. Level 3 MQSZS off-board charger for AC microgrid applications.

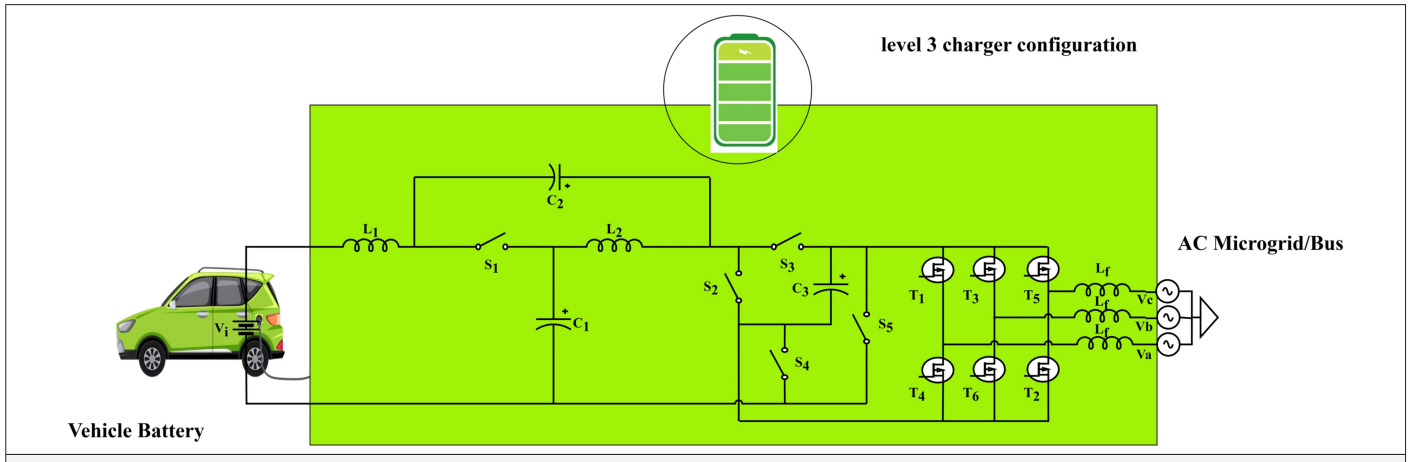

Fig. 2. Modified quasi switched Z-source configuration for vehicular applications.

III. POWER ANALYSIS FOR REFERENCE CURRENT GENERATION IN WEAK GRIDS

The generic voltages expression in (1) at the point of common coupling in terms of positive, negative, and zero sequence components denoted by +k, −k, and 0k for the kth order harmonic component of voltage vector *e*.

$$\check{e}=\sum_{k=1}^{\infty}\left(e^{+k}+e^{-k}+e^{0k}\right)$$

$$\check{e}=\sum_{k=1}^{\infty}\left\{E^{+k}\begin{bmatrix}\cos\left(k\omega t+\varnothing^{+k}\right)\\ \cos\left(k\omega t-2\pi/3+\varnothing^{+k}\right)\\ \cos\left(k\omega t+2\pi/3+\varnothing^{+k}\right)\end{bmatrix}+E^{-k}\begin{bmatrix}\cos\left(k\omega t+\varnothing^{-k}\right)\\ \cos\left(k\omega t-2\pi/3+\varnothing^{-k}\right)\\ \cos\left(k\omega t+2\pi/3+\varnothing^{-k}\right)\end{bmatrix}+E^{0k}\begin{bmatrix}\cos\left(k\omega t+\varnothing^{0k}\right)\\ \cos\left(k\omega t-2\pi/3+\varnothing^{0k}\right)\\ \cos\left(k\omega t+2\pi/3+\varnothing^{0k}\right)\end{bmatrix}\right\} \quad (1)$$

Similarly, expression in (2) represents the grid current vector *i* obtained in terms of sequential components n+ and n− as shown below.

$$\check{i}=\sum_{k=1}^{\infty}\left\{I^{+n}\begin{bmatrix}\sin\left(n\omega t+\delta^{+n}\right)\\ \sin\left(n\omega t-2\pi/3+\delta^{+n}\right)\\ \sin\left(n\omega t+2\pi/3+\delta^{+n}\right)\end{bmatrix}+I^{-n}\begin{bmatrix}\sin\left(n\omega t+\delta^{-n}\right)\\ \sin\left(n\omega t-2\pi/3+\delta^{-n}\right)\\ \sin\left(n\omega t+2\pi/3+\delta^{-n}\right)\end{bmatrix}\right\} \quad (2)$$

As per instantaneous power theory [19], the active and reactive powers are a dot product and a cross product of the interaction between generic voltage and current vectors.

$$\begin{bmatrix}p\\ q\end{bmatrix}=\begin{bmatrix}P_{c2} & P_{s2}\\ Q_{c2} & Q_{s2}\end{bmatrix}\begin{bmatrix}\cos(2\omega t)\\ \sin(2\omega t)\end{bmatrix}+\begin{bmatrix}P_0\\ Q_0\end{bmatrix} \quad (3)$$

As per [20], the complete power matrix in the synchronous reference frame for unbalanced or weak grid represented by (3).

$$\begin{bmatrix}P_0\\ P_{c2}\\ P_{s2}\\ Q_0\\ Q_{c2}\\ Q_{s2}\end{bmatrix}=\begin{bmatrix}e_d^{+} & e_q^{+} & e_d^{-} & e_q^{-}\\ e_d^{-} & e_q^{-} & e_d^{+} & e_q^{+}\\ e_q^{-} & -e_d^{-} & -e_q^{+} & e_d^{+}\\ e_q^{+} & -e_d^{+} & e_q^{-} & -e_d^{-}\\ e_q^{-} & -e_d^{-} & e_q^{+} & -e_d^{+}\\ -e_d^{-} & -e_q^{-} & e_d^{+} & e_q^{+}\end{bmatrix}\begin{bmatrix}i_d^{+}\\ i_q^{+}\\ i_d^{-}\\ i_q^{-}\end{bmatrix} \quad (4)$$

Calculating power converter-injected current in unbalanced grid conditions requires the use specific strategies. Slow charger dynamics, continuous power from the grid-tied converter, and disregarding zero sequence voltages are all assumptions. $\tilde{p}$ and $\tilde{q}$ are the oscillatory active and reactive power components, respectively. The orthogonal voltage vector $\hat{e}_{\perp}$ is 90° ahead of $\hat{e}$. The oscillating power terms are reduced when the formulation is simplified.

$$\tilde{p}=e^{+}.i_q^{-}+e^{-}.i_q^{+}+\underbrace{e^{+}.i_p^{*-}+e^{-}.i_p^{*+}}_{0}$$
$$\tilde{q}=e_{\perp}^{+}.i_p^{-}+e_{\perp}^{-}.i_p^{+}+\underbrace{e_{\perp}^{+}.i_q^{*-}+e_{\perp}^{-}.i_q^{*+}}_{0} \quad (5)$$

IV. CONTROL SCHEME FOR MODIFIED SWITCHED Z SOURCE OFF-BOARD CHARGER

Fig. 3 shows the overall control for MSQZS level 3 off-board charger configuration to deal with unbalanced operating conditions. The finite set predictive algorithm (Fig. 4) is an extensively used control method as it eliminates the need for modulators and PI controllers. The FS-MPC algorithm eliminates the 2ω power ripples in single-phase three-leg quasi-converter during unbalance effectively compared to PI control [21]. It has a long prediction horizon that improves the harmonic distortion and significantly reduces the computational burden around 50% by including two variables in the cost functions [22].

FS-MPC increases performance and stability with lower current distortion. Fig. 5 depicts the operating principle of the FS-MPC algorithm. Consider the current as a generic system variable sampled

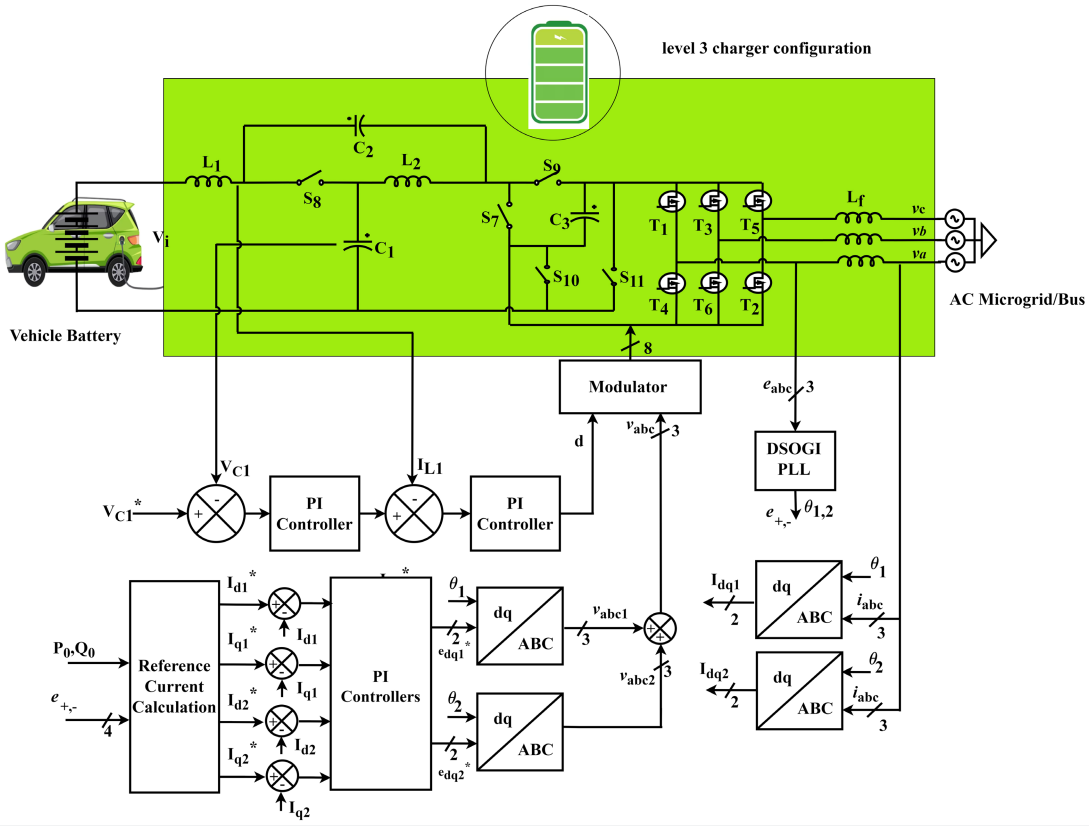

Fig. 3. Conventional proportional integral control scheme during unbalanced operating conditions.

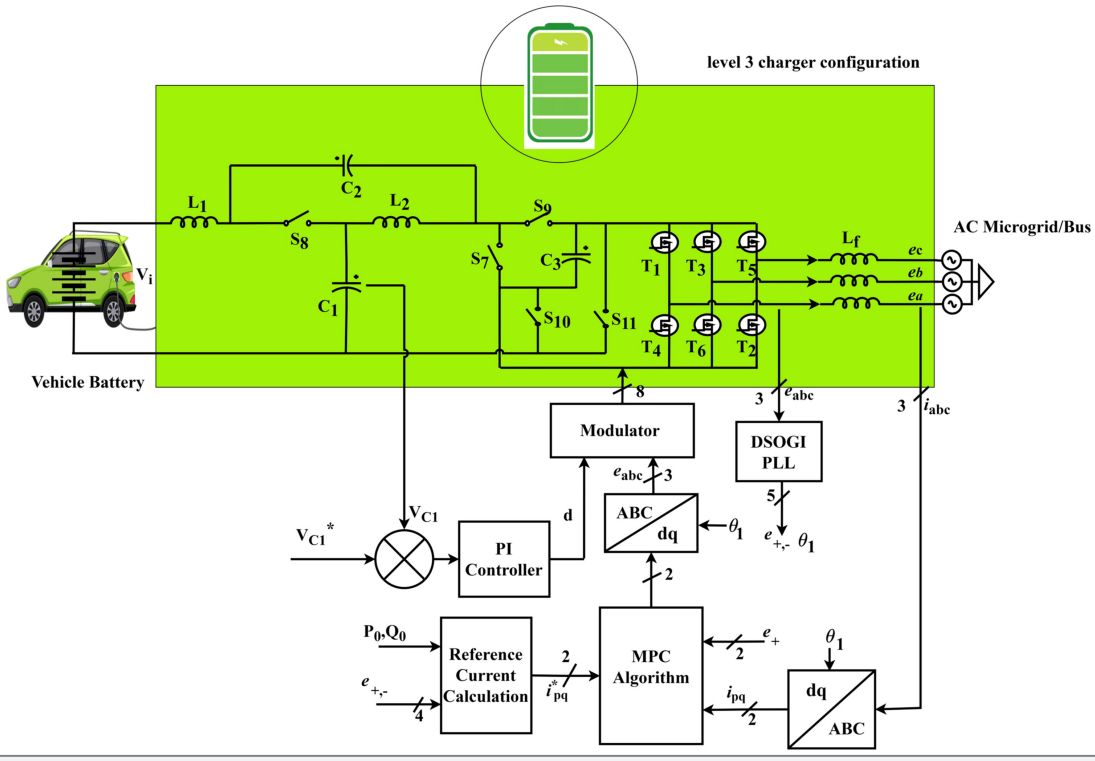

Fig. 4. Finite set predictive control algorithm for unbalanced operating conditions.

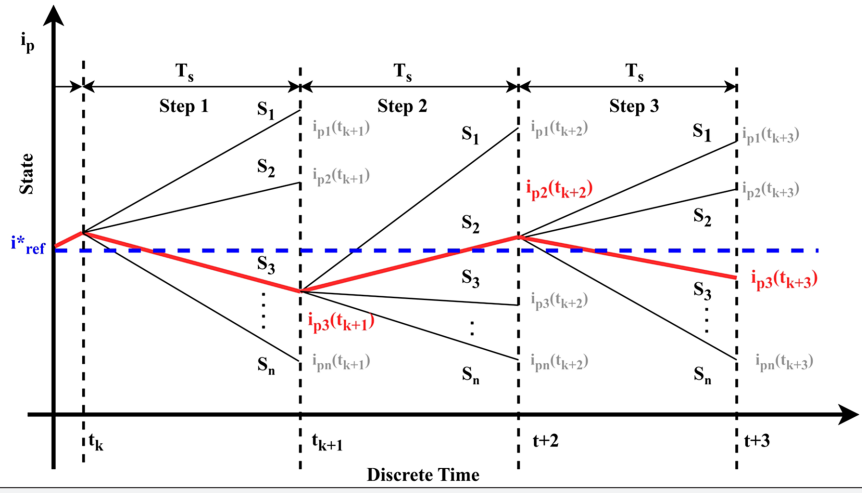

Fig. 5. Operating principle of finite set predictive algorithm [23].

over a period Ts with k as a finite number of control actions since control actions are finite in numbers denoted by Sn where n = 1 to m. The predictive current function $i_{pn}(t(k+1))$ depends on control actions and present measured value of current $i_p(t(k))$. The FS-MPC algorithm selects the function closest to the reference value such that the absolute error between the predictive function and the reference is minimum. Initial predictive value of grid current vectors obtained shown by the expression (6).

$$i_{d(m+1)} = \left(1 - \frac{R_f T_s}{L_f}\right) . i_{d(m)} + \frac{T_s}{L_f}\left\{V_{d(m)} - e_{d(m)} + \omega L_f . i_{q(m)}\right\}$$
$$i_{q(m+1)} = \left(1 - \frac{R_f T_s}{L_f}\right) . i_{q(m)} + \frac{T_s}{L_f}\left\{V_{q(m)} - e_{q(m)} - \omega L_f . i_{d(m)}\right\} \quad (6)$$

The quadratic cost function (7) can be written as follows:

$$C = C_d + C_q$$
$$C_d = \left|i_{d(ref)}^{*} - i_{d(m+1)}\right|^2 ; C_q = \left|i_{q(ref)}^{*} - i_{q(m+1)}\right|^2 \quad (7)$$

The above expression equates to zero upon partial differentiation gives the minimum value.

$$\frac{\partial C_d}{\partial V_{d(m)}} = 0$$
$$\frac{\partial C_q}{\partial V_{q(m)}} = 0 \quad (8)$$

The minimum grid voltage vector in DQ-domain derived from the (8) can be expressed as

$$V_{d,min} = \frac{L_f}{T_s}\left\{i^{*}_{d(ref)} - \left(1 - \frac{R_f T_s}{L_f}\right) . i_{d(m)}\right\} - \omega L_f . i_{q(m)} + e_{d(m)} \quad (9)$$

$$V_{q,min} = \frac{L_f}{T_s}\left\{i^{*}_{q(ref)} - \left(1 - \frac{R_f T_s}{L_f}\right) . i_{q(m)}\right\} + \omega L_f . i_{d(m)} + e_{q(m)} \quad (10)$$

These voltage vectors (9) and (10) in the synchronous reference frame using the Park's transformation generate the three-phase references for pulse width modulation that can further be compared with the switching signal to produce appropriate switching pulses for the MSQZSI configuration. Fig. 6 gives brief flow of the proposed predictive control algorithm below.

V. RESULTS AND DISCUSSION

In the EV context, Fig. 7(a) depicts a notable 20% A phase voltage drop with PI control, causing system imbalance, double-frequency ripples, and disruptive power oscillations. Traditional remedies involve six PI controllers, but precision wanes due to negative sequence currents. However, Fig. 7(b) shows the FS-MPC's effectiveness in curbing

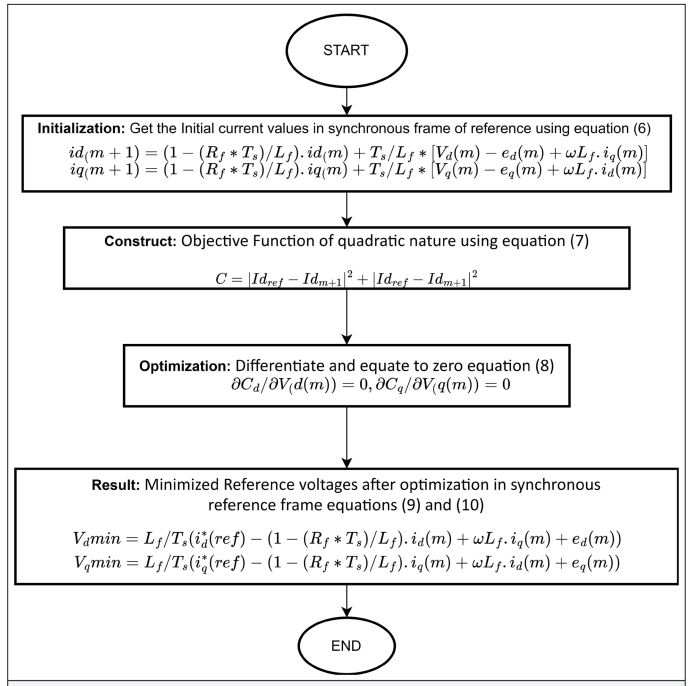

Fig. 6. Algorithm for model based predictive control strategy on novel modified switched Z source converter.

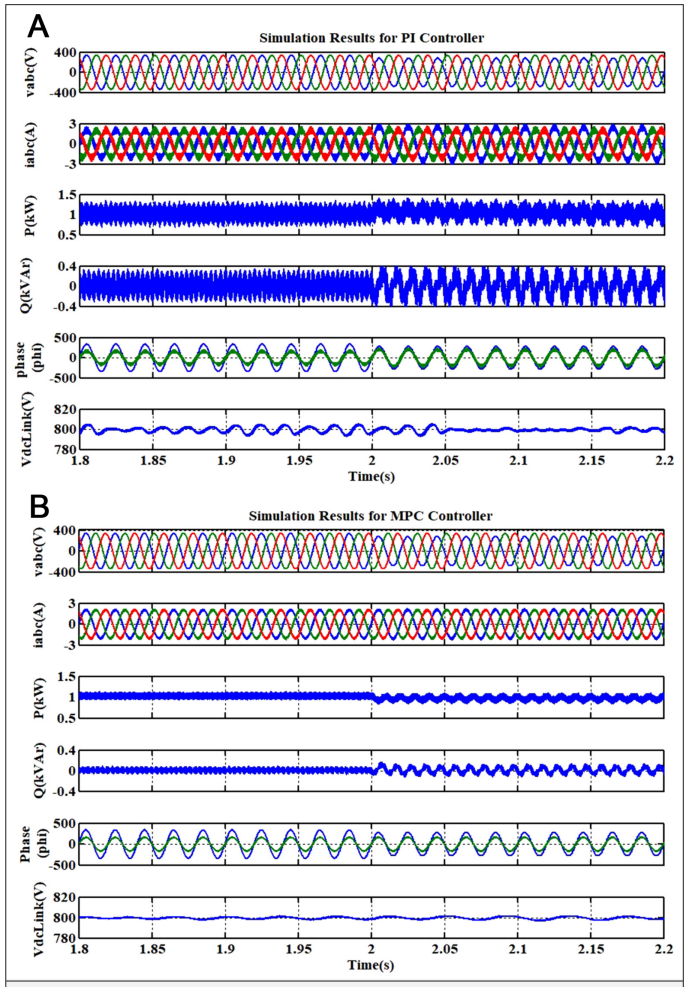

Fig. 7. Result analysis for (a) conventional PI control and (b) finite set predictive algorithm scheme under phase A unbalancing with 20% sag.

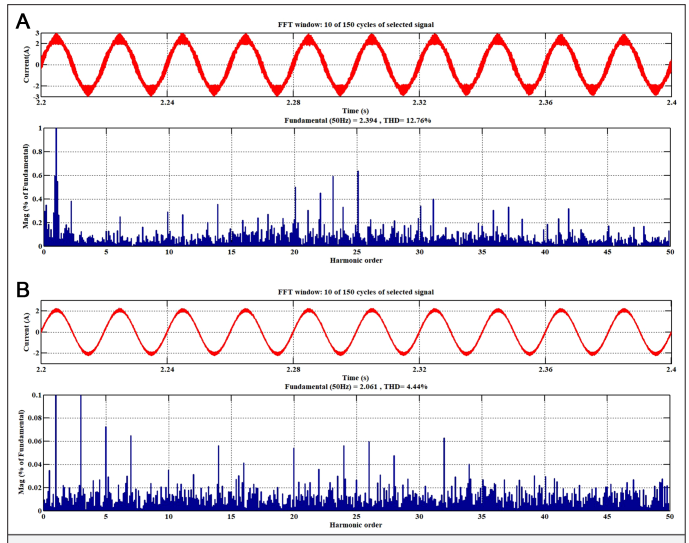

Fig. 8. FFT analysis of phase A current waveform for unbalanced grid voltages A with (a) conventional PI Control (b) finite set MPC.

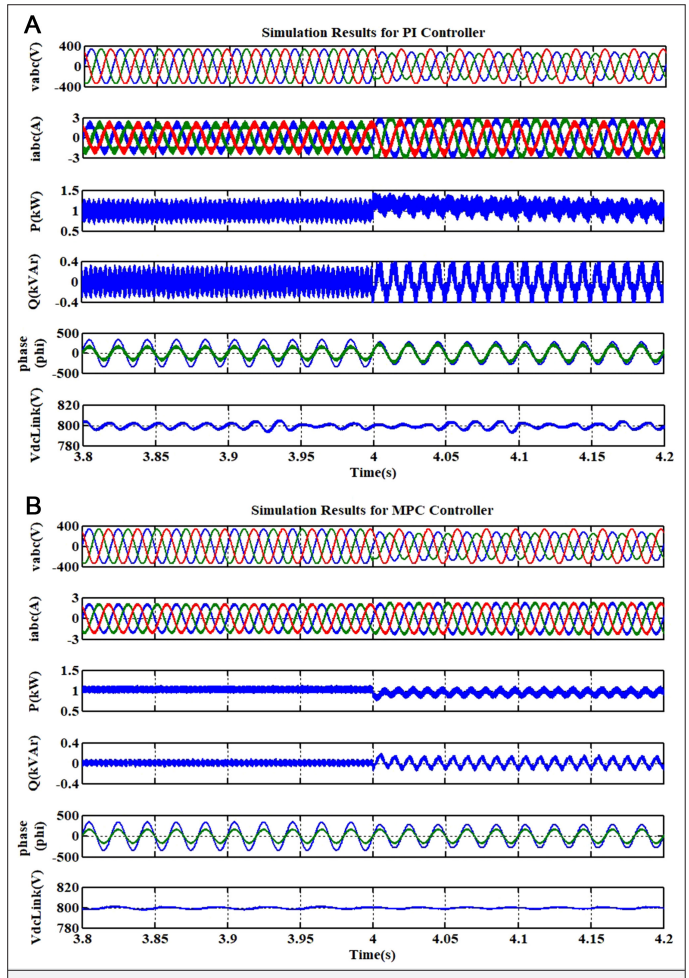

Fig. 9. Result analysis for (a) conventional PI control and (b) finite set predictive algorithm scheme under phase A and B unbalancing with 20% and 30% sag.

ripples and power oscillations without needing multiple loops or complex tuning during voltage imbalances. Regarding EV charging, Fig. 8(a) exposes phase A current waveform distortion with PI control, yielding a high 12.76% total demand distortion (TDD), breaching IEEE519™-2014 standards. Conversely, Fig. 8(b) demonstrates the predictive control's response to a 20% phase A voltage sag, yielding a TDD of 4.44%, within the acceptable range. Fig. 9(a) underscores the challenge of minimizing oscillatory power elements, even with six PI controllers, causing significant DC-link variations in the EV-charging system. Fig. 9(b) spotlights the FS-MPC's potential in reducing ripples and power oscillations in unbalanced grid voltages. Fig. 10(a) assesses power quality and reveals an alarming 12.22% TDD in phase A current waveform, surpassing IEEE519TM-2014 standards. However, Fig. 10(b) attains compliance with a 4.30% TDD, beneath the 5% threshold. Table I summarizes Fourier analyses, affirming FS-MPC's superiority in significantly reducing TDD levels from 12.76% to 4.44% during a 20% phase A voltage sag.

In the simulation, a uniform 10 µS sampling time, totaling 20 samples for a 5 kHz sampling frequency, ensured a fair PI controller and Finite-Control Set Model Predictive Control (FCS-MPC) comparison. Table II details various Z source topologies with distinct parameters, while Table III compares PI and FS-MPC, highlighting sample times

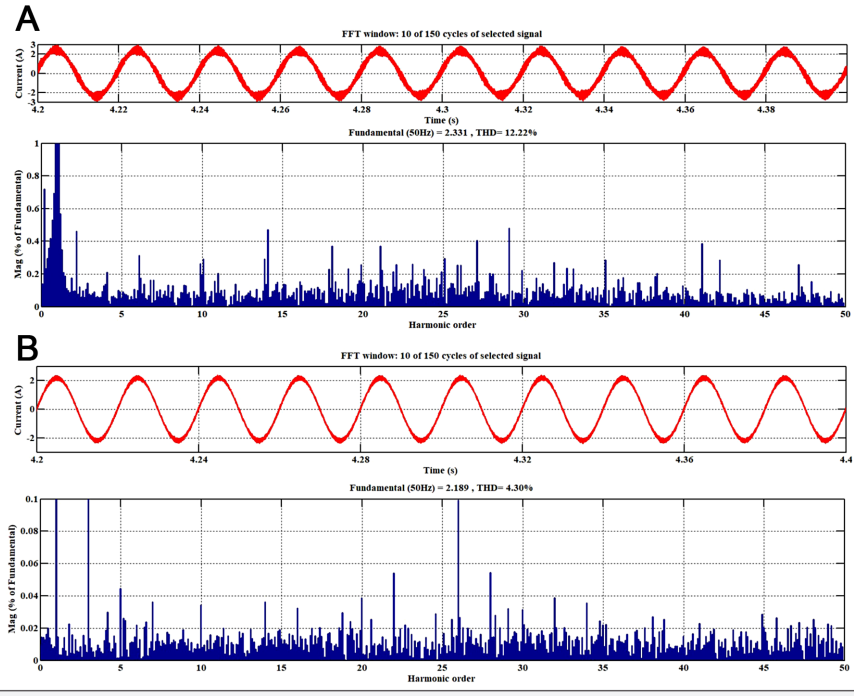

Fig. 10. FFT analysis of phase A current waveform for unbalanced grid voltages A and B with (a) conventional PI control (b) finite set MPC.

TABLE I. TABULATED RESULTS OF PHASE A CURRENT WAVEFORM FFT ANALYSIS UNDER DIFFERENT LEVEL OF UNBALANCING

		TDD Levels for Phase A Current	
S.N.	**Type of Unbalance**	**PI Control**	**Finite Set-MPC**
1	Sag of 20% in phase A voltage waveform	12.76%	4.44%
2	Sag of 20% in phase A and Sag of 30% in phase B voltage	12.22%	4.30%

TABLE II. COMPARISON FOR DIFFERENT Z SOURCE TOPOLOGY WITH MODIFIED SWITCHED Z SOURCE CONVERTER

		Different Types of Z Source Converters			
S.N.	**Parameters**	**Basic Z Source[24]**	**Quasi Z source [25]**	**Switched Z Source [26]**	**Modified Switched Z Source[18]**
1	Input voltage	$\frac{V_0}{1-2D}$	$\frac{V_0}{1-D}$	$\frac{V_0}{1-2D}$	$\frac{V_0}{1-4D}$
2	Voltage on capacitor C_1 (V_{C1})	$\frac{1-D}{1-2D}V_0$	$\frac{1-D}{1-2D}V_0$	$\frac{1-D}{1-2D}V_0$	$\frac{1-2D}{1-4D}V_0$
2	Voltage on capacitor C_2 (V_{C2})	$\frac{1-D}{1-2D}V_0$	$\frac{D}{1-2D}V_0$	$\frac{1-D}{1-2D}V_0$	$\frac{1-2D}{1-4D}V_0$
3	Voltage stress on the switches (V_{S1} and V_{S2})	$\frac{1-D}{1-2D}V_0$	$\frac{2D}{1-2D}V_0$	$\frac{1-D}{1-2D}V_0$	$\frac{1-2D}{1-4D}V_0$
4	Current stress on inductor L_1(I_{L1})	$\frac{I_0}{1-2D}$	$\frac{I_0}{1-2D}I_0$	$\frac{I_0}{1-4D}$	$\frac{I_0}{1-4D}$
5	Current stress on inductor L_2(I_{L2})	$\frac{I_0}{1-2D}$	$\frac{I_0}{1-2D}I_0$	$\frac{I_0}{1-4D}$	$\frac{I_0}{1-4D}$
6	Input current	$\frac{1}{1-2D}I_0$	$\frac{I_0}{1-2D}$	$\frac{I_0}{1-4D}$	$\frac{I_0}{1-4D}$
7	Constant DC link	NO	NO	NO	YES
8	Duty ratio	0<D<0.5	0<D<0.5	0<D<0.25	0<D<0.25

TABLE III. ANALYSIS BASED ON MATH OPERATIONS REQUIRED BY DIFFERENT CONTROL SCHEMES

		Complexity Analysis	
S.N.	**Parameters**	**Conventional Control Scheme**	**Finite Set Predictive Control Algorithm**
1	Main controller	PI Controller {[3(x)+5(+)] *2+1(+)} *6	Finite Set-MPC Algorithm{3(x)+3(+) +2(−)} *2
2	Type of block set required with quantity		
	PI controller:	06	01
	Transformation (Park's and Clark's):	04	02
	Phase lock loop:	01	01
3	Feed forward path:	Required	Not required
4	Cross coupling loop:	Required	Not required
5	Total math operations	{37(x)+28(+) +18(−)}	{20(x)+10(+) +6(−)}
6	Relative processing time	Very high	Low

Note: Each T_{dq} requires {6(x)+1(+) +1(−)}; each PI controller {2(x)+2(+)}; each cross-coupling loop: {2(x)+1(+)}; each feed forward path: 1(+)

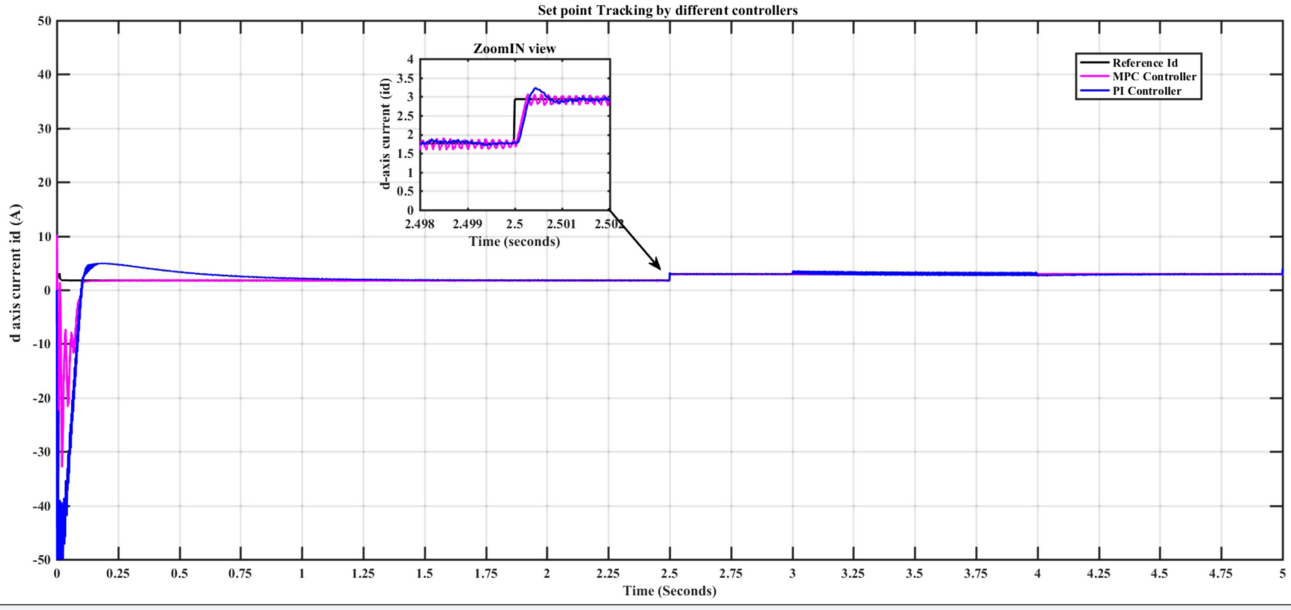

Fig. 11. Performance analysis of PI and FSMPC controllers during step change in reference current id.

and arithmetic operator usage. These results emphasize FCS-MPC's potential to tackle unbalanced grid voltages, improving EV charging system power quality, stability, and overall performance.

Fig. 11 illustrates the MPC controller's robust adaptability to a step change in the reference current id(ref), in contrast to the PI controller's tracking of the setpoint.

VI. CONCLUSION

Small distributed networks confront imbalance concerns in the context of electric vehicles (EVs) due to poorly linked loads and grid voltages with a low X/R ratio. These mismatches have an impact on EV charging infrastructure and performance. Traditional PI control suffers with negative sequence components, resulting in mediocre outcomes. Unbalanced grid voltages distort grid currents and interrupt the DC-Link voltage, compromising charging and EV stability. To solve this, the research provides a FS-MPC mechanism that minimizes negative sequence impact while remaining simple. Implementing it in EV charging infrastructure reduces grid voltage impacts and power oscillations, improving efficiency and stability. This paper highlights EV charging issues in small networks and proposes the FS-MPC approach as a possible alternative for increasing infrastructure performance and EV integration into sustainable energy systems.

Peer-review: Externally peer-reviewed.

Author Contributions: Concept – A.T., A.C.; Design – A.T., A.C.; Supervision – A.C.; Funding – A.C., A.T.; Materials – A.T., A.C.; Data Collection and/or

Processing – A.C., A.T.; Analysis and/or Interpretation – A.T., A.C.; Literature Review – A.C., A.T.; Writing – A.T., A.C.; Critical Review – A.C., A.T.

Declaration of Interests: The authors have no conflicts of interest to declare.

Funding: The authors declared that this study has received no financial support.

REFERENCES

1. U. Datta, A. Kalam, and J. Shi, "A review of key functionalities of battery energy storage system in renewable energy integrated power systems," *Energy Storage*, vol. 3, no. 5, p. e224, 2021. [CrossRef]
2. O. M. Toledo, D. Oliveira Filho, and A. S. A. C. Diniz, "Distributed photovoltaic generation and energy storage systems: A review," *Renew. Sustain. Energy Rev.*, vol. 14, no. 1, pp. 506–511, 2010. [CrossRef]
3. P. Saini, and L. Gidwani, "An investigation for battery energy storage system installation with renewable energy resources in distribution system by considering residential, commercial and industrial load models," *J. Energy Storage*, vol. 45, p. 103493, 2022. [CrossRef]
4. Y. Ren, S. J. Rind, and L. Jiang, "A coordinated control strategy for battery/supercapacitor hybrid energy storage system to eliminate unbalanced voltage in a standalone AC microgrid," *J. Intell. Manuf. Spec. Equip.*, vol. 1, no. 1, pp. 3–23, 2020. [CrossRef]
5. S. B. Wali *et al.*, "Battery storage systems integrated renewable energy sources: A biblio metric analysis towards future directions," *J. Energy Storage*, vol. 35, p. 102296, 2021. [CrossRef]
6. C. S. Jardim, *The Effective Load Carrying Capacity of Grid-Connected Photovoltaic Systems as a Peak Shaving Tool in Daytime Peaking Feeders in Urban Areas* PhD Thesis. Graduate Program of Civil Engineering, 2007.
7. D. K. Nichols, and S. Eckroad, "Utility-scale application of sodium sulfur battery," in Proc. 7th Annu. Int. Stat. Battery Conf. (Battcon'03), Marco Island, FL, USA, 2003, pp. 28–30.
8. S. Y. Hussain, and K. R. Rani, "Z-source inverter for RES-EVS with flexible energy control functions,", in *Smart and Intelligent Systems*. Berlin: Springer, 2022, pp. 187–194. [CrossRef]
9. Y. Huang, M. Shen, F. Z. Peng, and J. Wang, " Z -Source inverter for residential photovoltaic systems," *IEEE Trans. Power Electron.*, vol. 21, no. 6, pp. 1776–1782, 2006. [CrossRef]
10. A. Tiwari, and A. Chowdhury, "Bi-q MSZSI topology for grid-tied inverter under ideal grid conditions," in *Sustainable Technology and Advanced Computing in Electrical Engineering: Proceedings of ICSTACE*. Berlin: Springer, 2022, pp. 73–82. [CrossRef]
11. A. Laib, F. Krim, B. Talbi, and A. Sahli, "A predictive control scheme for large-scale grid-connected PV system using high-level NPC inverter," *Arab. J. Sci. Eng.*, vol. 45, no. 3, 1685–1701, 2020. [CrossRef]
12. L. Liu, H. Li, Y. Xue, and W. Liu, "Decoupled active and reactive power control for large-scale grid-connected photovoltaic systems using cascaded modular multilevel converters," *IEEE Trans. Power Electron.*, vol. 30, no. 1, 176–187, 2015. [CrossRef]
13. V. Yaramasu, B. Wu, and J. Chen, "Model-predictive control of grid-tied four-level diode-clamped inverters for high-power wind energy conversion systems," *IEEE Trans. Power Electron.*, vol. 29, no. 6, 2861–2873, 2014. [CrossRef]
14. V. Yaramasu, and B. Wu, "Model predictive decoupled active and reactive power control for high-power grid-connected four-level diode-clamped inverters," *IEEE Trans. Ind. Electron.*, vol. 61, no. 7, 3407–3416, 2014. [CrossRef]
15. M. Yilmaz, and P. T. Krein, "Review of battery charger topologies, charging power levels, and infrastructure for plug-in electric and hybrid vehicles," *IEEE Trans. Power Electron.*, vol. 28, no. 5, 2151–2169, 2013. [CrossRef]
16. A. Tiwari, and A. Chowdhury, "An Indirect PI-MPC Hybrid Method-Based Bi-quasi-Modified Switched Z Source Inverters for Vehicle to Grid applications," *Electrica*, 2022. [CrossRef]
17. H. Shen, B. Zhang, and D. Qiu, "Hybrid Z-source boost DC–DC converters," *IEEE Trans. Ind. Electron.*, vol. 64, no. 1, pp. 310–319, 2016. [CrossRef]
18. A. Tiwari, and A. Chowdhury, "Modified switched Z-source topology for inverter applications," in *Proceedings of Symposium on Power Electronic and Renewable Energy Systems Control*. Berlin: Springer, 2021, pp. 31–41. [CrossRef]
19. R. Teodorescu, M. Liserre, and P. Rodriguez, *Grid Converters for Photovoltaic and Wind Power Systems*. Chichester, UK: John Wiley & Sons, 2011.
20. S. Revelo, and C. A. Silva, "Current reference strategy with explicit negative sequence component for voltage equalization contribution during asymmetric fault ride through," *Int. Trans. Electr. Energy Syst.*, vol. 25, no. 12, pp. 3449–3471, 2015. [CrossRef]
21. R. Alla, and A. Chowdhury, "Model predictive controller for improved hybrid three quasi Z source inverter for DG applications," in 2018 IEEE Int. Conf. Power Electron., Drives Energy Sys. (PEDES), Vol. 2018, 2018, pp. 1–6. [CrossRef]
22. Y. Liu, B. Ge, H. Abu-Rub, H. Sun, F. Z. Peng, and Y. Xue, "Model predictive direct power control for active power decoupled single-phase quasi-Z-source inverter," *IEEE Trans. Industr. Inform.*, vol. 12, no. 4, pp. 1550–1559, 2016.
23. S. Kouro, P. Cortés, R. Vargas, U. Ammann, and J. Rodríguez, "Model predictive control—A simple and powerful method to control power converters," *IEEE Trans. Ind. Electron.*, vol. 56, no. 6, pp. 1826–1838, 2008. [CrossRef]
24. F. Z. Peng, "Z-source inverter," *IEEE Trans. Ind. Appl.*, vol. 39, no. 2, pp. 504–510, 2003.
25. J. Anderson, and F. Z. Peng, "Four quasi-Z-source inverters," in 2008 IEEE Power Electronics Specialists Conf., Vol. 2008, 2008, pp. 2743–2749. [CrossRef]
26. J. Liu, J. Wu, J. Qiu, and J. Zeng, "Switched Z-source/quasi-Z-source DC-DC converters with reduced passive components for photovoltaic systems," *IEEE Access*, vol. 7, pp. 40893–40903, 2019. [CrossRef]

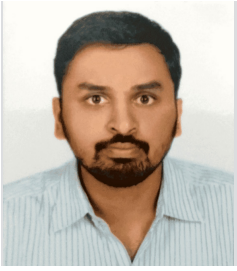

Anish Tiwari received the B.E. Electrical and Electronics degree from Rajiv Gandhi Proudyogiki Vishwavidyalaya, Bhopal, India, in 2012 and M.E. Power Systems from UIT-RGPV Bhopal India in 2015. Currently, he is pursuing a Doctoral degree in Electrical Engineering at Sardar Vallabhbhai National institute of technology Surat, India, from December 2018. His current research area includes Electric vehicle, Power Converters, and their applications, Power electronics, and impedance source networks.

Anandita Chowdhury received her B.E. and M.E. degrees from the University of Calcutta and her Ph.D. degree from the Indian Institute of Technology, Kharagpur. Presently, she is working as a Professor in the Department of Electrical Engineering of S. V. National Institute of Technology, Surat, India. She has more than twenty-five years of teaching experience. Her areas of research interest include electrical machines, drives, and power system stability.